



Article

Grain Refinement of Pure Magnesium for Microforming Application

Siska Titik Dwiyati , Gandjar Kiswanto * and Sugeng Supriadi

Department of Mechanical Engineering, Universitas Indonesia, Kampus UI, Depok 16424, Indonesia; siska.titik@ui.ac.id (S.T.D.); sugeng@eng.ui.ac.id (S.S.)

* Correspondence: gandjar_kiswanto@eng.ui.ac.id

Abstract: Magnesium is a suitable candidate material for temporary implant applications, such as a miniplate, due to its biocompatibility, density, and elastic modulus comparable to that of human bone. The biodegradability property of magnesium can minimize the need for a second surgery after the healing process, thereby reducing costs and pain for patients. On the other hand, microforming is a promising technology for manufacturing miniplates with high production rates and good mechanical properties. However, the application of magnesium in microforming is limited and remains a challenge in resolving issues related to the size effect in microforming and the low formability of magnesium, especially at room temperature. Grain refinement and homogenization are alternative approaches to controlling the size effect in magnesium microforming and improving formability. As the grain refinement process influences the mechanical and corrosion behavior of magnesium, this research shows that the grain refinement process for pure magnesium improves the overall performance of the microforming process for implant applications.

Keywords: grain refinement; microforming; pure magnesium



Citation: Dwiyati, S.T.; Kiswanto, G.; Supriadi, S. Grain Refinement of Pure Magnesium for Microforming Application. *J. Manuf. Mater. Process.* **2023**, *7*, 140. <https://doi.org/10.3390/jmmp7040140>

Received: 2 July 2023

Revised: 28 July 2023

Accepted: 1 August 2023

Published: 4 August 2023



Copyright: © 2023 by the authors. Licensee MDPI, Basel, Switzerland. This article is an open access article distributed under the terms and conditions of the Creative Commons Attribution (CC BY) license (<https://creativecommons.org/licenses/by/4.0/>).

1. Introduction

The research on medical implants has reached a third generation, which has gained significant interest and is currently undergoing intensive development in biodegradable materials for fracture fixation [1]. Among various metallic biodegradable materials, magnesium stands out as a promising candidate for temporary implants, such as miniplates, due to its biocompatibility, comparable density, and elastic modulus to human bone and its role as an essential component for metabolism [2]. The utilization of magnesium can minimize the need for a second surgery to remove the implant after the healing process, thus reducing costs and alleviating patient discomfort [3]. However, the application of magnesium as a biodegradable implant has issues due to its low strength and ductility, coupled with a high corrosion rate [4].

Improvements in the mechanical properties and corrosion resistance of magnesium have been achieved through alloying with other essential elements [5,6]. Rare earth, aluminum, and other elements with lower biocompatibility have been studied to enhance mechanical properties [6–8]. However, to prevent contamination and minimize side effects on the human body, the preference lies in the use of pure magnesium. Another method to enhance the mechanical properties and corrosion resistance of magnesium is through plastic deformation. Plastic deformation proves to be an effective approach for pure magnesium as it leads to grain refinement, resulting in improved strength according to the Hall–Petch equation and resistance to dislocation movement through grain boundary strengthening [9,10]. The influence of the grain refinement process and grain size on the corrosion susceptibility of magnesium was conducted by Ralston et al. Grain refinement appears to increase the corrosion resistance of magnesium alloys, primarily due to an improvement in passive film formation and adhesion resulting from increased grain boundary density.

However, it is worth noting that some reports have indicated that grain refinement could also lead to a decrease in corrosion resistance and accelerate the corrosion process [11]. This is because, in addition to grain refinement, other factors such as surface roughening, texture modification, formation of high-density dislocations, induction of residual stress, dissolution of second phases, and contaminant pickup are often present and can influence the overall corrosion behavior [12].

There are two types of plastic deformation methods, conventional deformation and severe plastic deformation (SPD). Conventional deformation processes like drawing, cold rolling, and extrusion can cause significant plastic strains, which in turn refine the grain structure [13]. However, in these conventional processes, an increase in strength is often accompanied by a reduction in ductility. On the other hand, in the SPD method, the material is formed under high hydrostatic pressure, resulting in large deformations and high dislocation densities without causing any significant change in the material's dimensions. SPD has the ability to more effectively refine the grain structure. The most common technique used for SPD is equal channel angular pressing (ECAP). The ECAP process involves pressing the specimen through dies comprising two intersecting channels, resulting in a deformation angle. During ECAP, the applied pressure induces plastic deformation in the material, leading to grain refinement, as well as an increase in the material's strength and ductility [14]. Processing magnesium using ECAP is not straightforward. This is mainly due to the inherent brittleness of magnesium. As a result, processing is usually carried out at high temperatures to make the material more malleable and easier to work with during ECAP. However, the mechanism of grain refinement in magnesium may lead to a heterogeneous grain structure with a multi-modal grain size distribution [15].

Recently, magnesium miniplates have been mainly manufactured through machining. However, microforming is a promising alternative with high mechanical properties, productivity, and cost-effectiveness by minimizing material waste. Microforming is the process of manufacturing parts in the submillimeter range through plastic deformation [16]. The microforming process for miniplate includes microshearing, which consists of microblanking and micropunching. The shearing process involves elastic and plastic deformation, as well as the fracture of the metal sheet between the punch and die. Material separation occurs in the cutting zone when the shear stress reaches the ultimate shear strength [17]. The geometry of the shear edge in microshearing is an indicator of product quality. The larger or higher the smooth and shiny shear zone surface and the smaller the fracture surface and burr, the better the quality of the microshearing result. This depends on several parameters, including punch-die clearance, punch-die corner radius, punchspeed, material properties, tool wear, misalignment, and temperature [18].

So far, the research trend in magnesium microforming primarily focuses on elevated temperatures, which provide a homogenizing effect suitable for controlling size effects and reducing scattering [19]. Furthermore, the magnesium process at elevated temperatures enhances the activation of non-basal slip, which can induce the dynamic recrystallization (DRX) process and improve formability [20]. However, the undesirable grain growth that occurs above a certain temperature should be carefully considered. Kim et al. conducted an investigation on the microforging of a magnesium alloy using V-grooved dies. The AZ91 alloy underwent refinement through differential speed rolling (HRDSR), resulting in fine grains that exhibited remarkable superplasticity and formability at temperatures ranging from 220 °C to 300 °C. However, at 300 °C, formability decreased due to grain growth [21]. Su et al. conducted a study on the microembossing process of ultrafine-grained LZ91 Mg-Li to produce micro-array channels with widths ranging from 50 to 200 µm. The channels were found to be influenced by temperature and grain size. The presence of an ultrafine-grained structure led to smooth and high-quality filling at a temperature of 150 °C [22].

Therefore, to bring the microforming process to room temperature, several challenges need to be addressed, including the size effect in microforming and the low formability of magnesium [23]. One alternative approach to tackle these challenges is grain refinement using the ECAP process. Grain refinement enhances grain boundary sliding and facilitates

further deformation, thus improving formability, as studied by Biswas [24]. However, it is essential for the grain refinement process not only to result in finer grains but also to achieve homogeneity to prevent scattering due to the size effect.

A new method employed to homogenize the ECAP microstructure distribution is recrystallization. However, during the recrystallization process, the growth of new grains may occur, which is determined by temperature, degree of deformation, and time. Zhu et al. stated that stored energy plays a key role in controlling recrystallization [25]. Song et al. found that high stored energy can promote recrystallization nucleation and inhibit grain coarsening during the recrystallization process [26]. Moreover, the higher the deformation experienced, the lower the recrystallization temperature required. Increasing the temperature results in a decrease in the crystal lattice's stiffness, leading to grain growth. Furthermore, fine grains exhibit more significant recrystallization compared to coarse grains due to the dominance of grain boundary nucleation [27].

In this research, a combination of magnesium grain refinement using ECAP and recrystallization was conducted to homogenize and reduce the size effect in microforming. The study also investigated its influence on mechanical properties and corrosion resistance for microforming applications.

2. Materials and Methods

A cast ingot of commercially pure Mg (99.8%) with the chemical composition shown in Table 1 was used as the starting material for the work, with a grain size of 632 μm . Specimens were prepared through equal channel angular pressing (ECAP) with up to eight passes.

Table 1. The composition of pure magnesium.

Element	Mg	Zn	Mn	Cu	Sn	Ca	Cd	Sr	Be
Wt (%)	99.8	0.039	0.037	0.020	0.018	0.015	0.001	0.0008	0.0002

The ECAP specimens were cylindrical billets measuring 11.87 mm in diameter and 65.88 mm in length. The ECAP process involves inserting the specimens into dies through a special channel with an intersecting angle of 120° , as shown in Figure 1. During the ECAP process, the specimens were heated to a temperature of 300°C while applying a pressure of 2500 kN. The process was repeated for two, six, and eight passes. In the subsequent repetitions, the specimens underwent a change in direction compared to the previous process, following route Bc, where the billet was rotated in a clockwise direction by 90° to the longitudinal axis between consecutive passes.

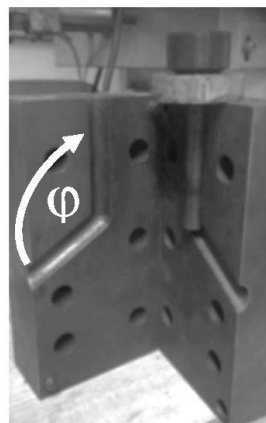


Figure 1. ECAP die with an angle ϕ of 120 degrees.

Subsequently, the recrystallization process after ECAP was carried out by heating the specimens in a vacuum tube furnace at a temperature of 200°C for 30 min.

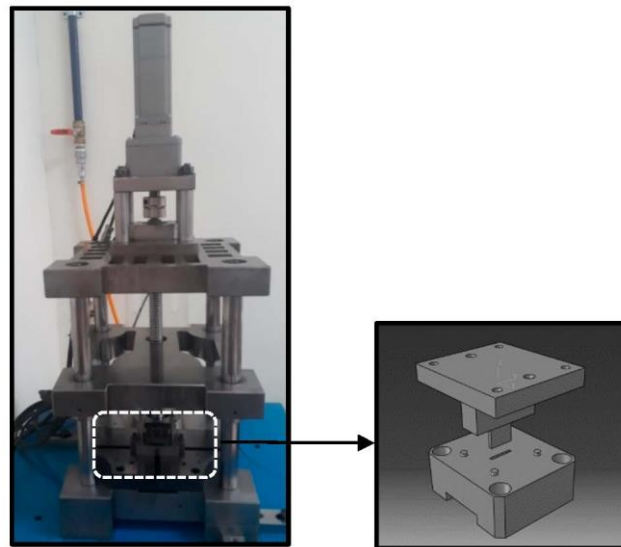


Figure 3. A 5 kN microforming machine and microblanking tool.

Table 2. Tooling and experimental parameters.

Parameters	Values
Punch-die material	SKD 11, HRC 63, non-coating
Punch maximum travel	2.5 mm
Punch dimension	Rectangular 1×7.45 mm Circular $d = 1.5$ mm
Workpiece thickness (t)	0.5 mm
Punch-die clearance (c)	0.01 mm
Punch velocity	7 mm/s
Temperature	27 °C

3. Results and Discussion

3.1. ECAP Process

The ECAP process is a severe plastic deformation process in which the material shaping is performed under high hydrostatic pressure, resulting in significant deformation. During this plastic deformation process, there is no change in the dimensions of the specimen. The specimens resulting from the ECAP process are shown in Figure 4.

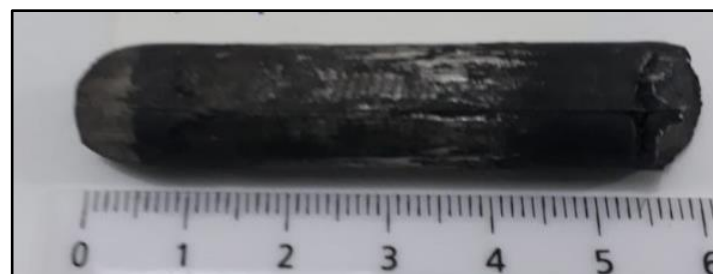


Figure 4. The result of the ECAP process.

The ECAP process was conducted at a temperature of 300 °C to accommodate deformation through the activation of non-basal slip systems. The presence of proper critical strain during high-temperature deformation will result in dynamic recrystallization. The representative image of the grain structure of the material in the as-cast condition and the

ECAP process with two passes are displayed in Figure 5. The image showed coarse grains as the initial microstructures.

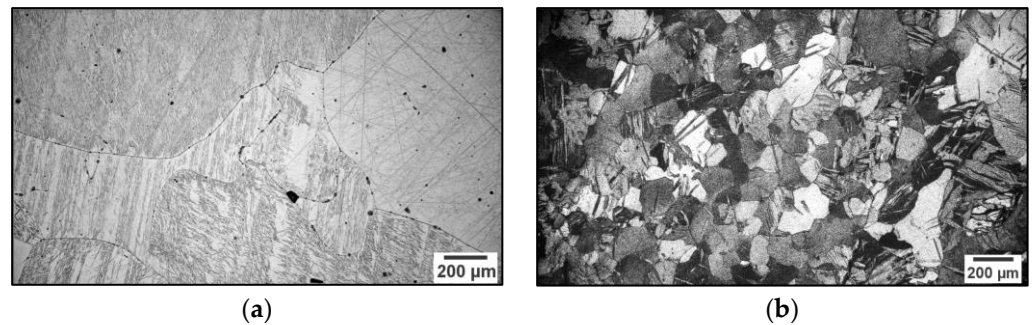


Figure 5. Microstructure of magnesium (a) as received and (b) ECAP 2 pass.

During the ECAP process with two passes, the magnesium undergoes a transformation where fine grains are formed, exhibiting an average grain size smaller than the as-received magnesium. However, this dynamic recrystallization process falls short of perfection as coarser grains can still be observed, resulting in a heterogeneous distribution. This occurrence is attributed to the insufficient strain experienced during the two-pass ECAP process, preventing complete recrystallization. By increasing the number of ECAP passes, the repeated deformation introduces additional strain that proves beneficial in achieving a more flawless recrystallization process and a greater quantity of finely shaped equiaxed grains.

The number of ECAP passes varied for each specimen. Figure 6 shows the grain size obtained after two, six, and eight passes of ECAP, compared to magnesium in its as-received (0 passes) condition. The most significant grain refinement occurred during the ECAP two-pass process, reducing the size from 632 μm to 115 μm . The grain size increases from two passes to six passes. This is because the deformation strain experienced is not sufficient to inhibit grain growth during the ECAP process at a temperature of 300 $^{\circ}\text{C}$.

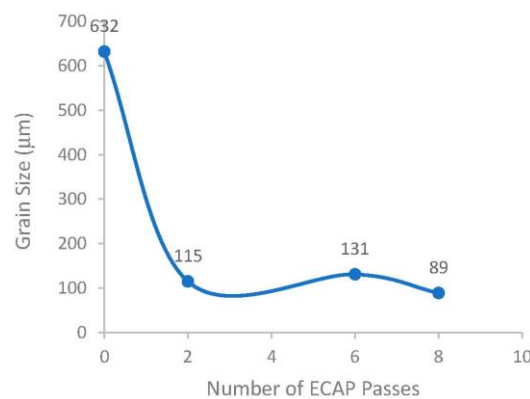


Figure 6. The effect of passes on the grain size of pure magnesium.

As the number of passes increases, the deformation becomes more significant, leading to the prominence of dynamic recrystallization and grain refinement in ECAP eight-pass, which effectively hinders grain growth. Consequently, the grain size resulting from the ECAP eight-pass processes is finer in comparison to that of the ECAP six-pass.

The number of passes in the ECAP process is related to the equivalent strain, which causes grain boundary pinning, resulting in finer grains. The grain refinement process can be analogized as a repeated process of dynamic recovery and recrystallization in each pass. The eight-pass ECAP process leads to dynamic recrystallization, resulting in a highly homogeneous grain distribution with the difference in grain size across various regions

of the specimen reaches a minimum. The plastic deformation process during the eight-pass ECAP generates an intense strain of 5.36, causing the grain boundaries to become less distinct.

Upon examining the grain size distribution resulting from the ECAP process, it becomes evident that there are variations in grain size observed in the outer, middle, and central regions of the specimens corresponding to 0, 2.5, and 5 mm distance from the specimen surface edge, as depicted in Figure 7. Despite undergoing multiple repetitions of the process, the distribution of grain sizes remains heterogeneous, and coarse grains persist. Notably, the grain size in the outer region of the specimen appears finer due to displacement against the die wall during the ECAP process. Conversely, the central region exhibits the largest grain size, indicating a relatively lower strain experienced and longer storage temperature by this part of the specimen. With an increasing number of passes, the level of heterogeneity diminishes.

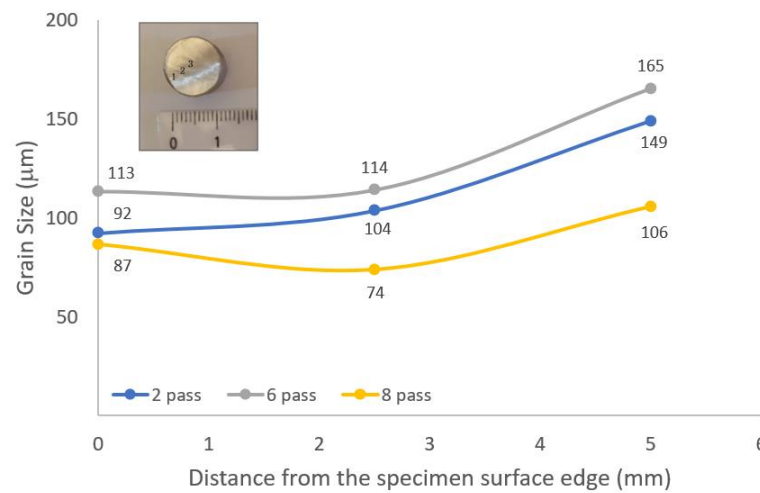


Figure 7. The grain size distribution resulting from ECAP.

Figure 8 displays the microstructure resulting from each ECAP pass observed at the edge, middle, and center of the specimen. The non-homogeneous grain size distribution in the ECAP process is a consequence of conducting the process at a temperature of 300 °C. Within the ECAP microstructure, twins are observed, leading to a significant increase in ductility.

		Observation Point (mm)		
		0	2.5	5
Number of ECAP Passes	2			
	6			
	8			

Figure 8. The grain size distribution in the microstructure of the ECAP-treated specimens.

3.2. The Influence of the ECAP Process on Mechanical Properties

Figure 9 shows the influence of the number of ECAP passes of pure magnesium on mechanical properties, and the corresponding results are shown in Table 3. In the ECAP two-pass specimen, there is a decrease in ductility compared to the as-received state, despite grain refinement. In contrast, the ECAP six and eight-pass specimens exhibit an increase in ductility by 22% (from 18 to 22) and 83% (from 18 to 33), respectively. The increase in ductility is particularly significant for the ECAP eight-pass specimens. The ECAP eight-pass experience a more dominant rotation of the basal planes and activation of non-basal planes, further enhanced by the presence of a large number of twinning. This study also supports the findings of Hakimian et al. [30].

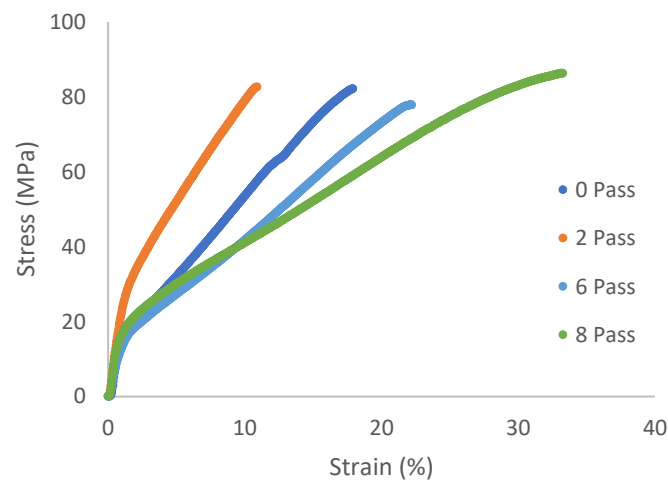


Figure 9. The stress-strain curve of the specimens resulting from the ECAP process.

Table 3. The mechanical properties resulted from the ECAP process.

Pass of ECAP	% EL	σ_y (MPa)	UTS (MPa)	Density (g/cm ³)
0	18	18	82	1.73
2	11	33	83	1.75
6	22	19	78	1.72
8	33	23	86	1.78

According to the Hall–Petch equation, the yield strength in ECAP two, six, and eight passes increases with grain refinement compared to the as-received state, with respective increases 83%, 6%, and 28% in ECAP two, six, and eight passes. The smallest increase in yield strength occurs in the ECAP six-pass, corresponding to its larger grain size.

Dynamic recrystallization during the ECAP process not only leads to grain refinement but also results in the formation of a weak basal texture. The specific texture plays a significant role in strength despite grain refinement. The mechanical strength shows only a modest increase with the ECAP process. The tensile strength increases by 1.2% (from 82 to 83 MPa) and 5% (from 82 to 86 MPa) for the ECAP 2 and eight-pass specimens, respectively. The fine grain size contributes to strengthening through grain boundary strengthening, which hinders dislocation movement, although the effect is not significant due to the evolution of a weak texture. On the contrary, in the ECAP six-pass, the strength decreases compared to the as-received magnesium. A similar phenomenon was observed by Tong et al., 2019, where mechanical strength decreased due to grain refinement resulting in a weak texture after the ECAP process [10].

Tensile testing was conducted using specimens with a thickness of 0.5 in accordance with the DIN 50125:2009-07 H standard. The tensile testing observed a size effect, where the elongation of the as-received magnesium increased from 9.1% to 18% in the testing

conducted using the ASTM E8 standard. However, the tensile strength values were almost the same, namely 73.5 compared to 82 MPa.

Table 3 shows the density of ECAP specimens. The data indicate a relationship between density and grain size in the results of ECAP. ECAP two and eight-pass specimens, which have finer grain sizes than ECAP six-pass, exhibit higher density. However, the density of ECAP six-pass is lower compared to the as-received condition due to defects in the specimen caused by high deformation during the ECAP process.

3.3. Annealing Process

During the ECAP process, the grain boundaries are at a high energy level due to the increasing formation ratio. This is because the number of dislocations accumulates at the grain boundaries and hinders further plastic deformation. To restore the formability properties, an annealing process can be performed. During the recrystallization stage, new grains start to grow homogeneously at the triple points of the previous grain boundaries, and dislocations can be eliminated due to atomic diffusion.

Annealing was conducted on the ECAP two-pass specimens. As seen in Figure 10, the grain size distribution at the surface edge, center, and core, corresponding to 0, 2.5, and 5 mm distance from the specimen surface edge, is shown. The grain size distribution of the ECAP two-pass specimens, as well as the ECAP specimens annealed at 200 °C and 250 °C for 30 min, can be observed in the figure. The annealing process on the ECAP two-pass specimens at 200 °C resulted in an average grain size of 56 μm (at the surface edge 50 μm, center 50 μm, and core 67 μm) and a more homogeneous microstructure. On the other hand, annealing at 250 °C produced finer grains, with an average grain size measuring 39 μm (at the outer 25 μm, middle 25 μm, and inner parts 68 μm), but with less homogeneous distribution in each part. The heterogeneity in grain size and distribution in materials is one of the factors that cause scattering in materials and microforming products due to the size effect. Homogenization can be improved with temperature and time, but it will decrease if grain growth occurs.

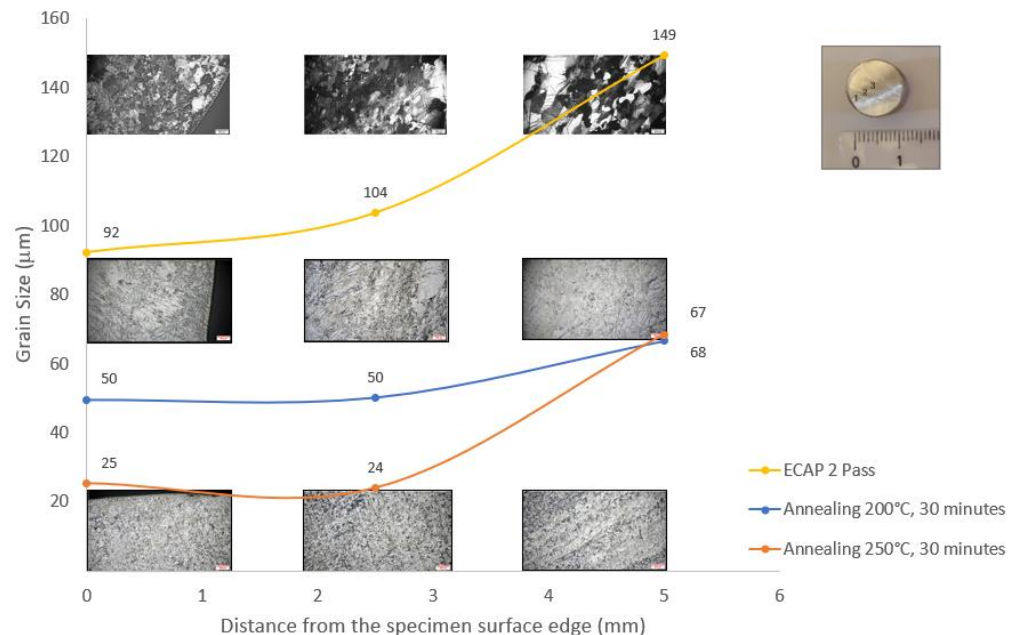


Figure 10. The grain size distribution of the annealed ECAP specimen.

The grain size produced is highly determined by the degree of deformation. With an increasing forming ratio, the size of the newly generated grains becomes smaller. Process parameters such as recrystallization temperature, heating rate, or the size of grains before formation can be disregarded compared to the degree of deformation. The critical deforma-

tion level varies for each material. If the degree of deformation is not sufficient for primary recrystallization, existing grain boundaries can shift, leading to local grain growth. Additionally, since the formation of new grains occurs at grain boundaries, finer grains provide more grain boundaries for grain refinement in the dynamic recrystallization process.

Figure 11 depicts the influence of annealing on the mechanical properties of the ECAP two-pass specimen. The mechanical strength increased by 59% (from 83 MPa to 132 MPa), and the ductility increased by 173% (from 11% to 30%) after the annealing process. The interaction between dislocations and twins enhanced the plastic deformation capacity of the annealed magnesium ECAP two-pass, leading to an increase in both tensile strength and strain. The remarkable ductility resulting from the annealing process becomes evident in the fracture of the tensile test specimen depicted in Figure 12. This specimen not only demonstrates ductility but also highlights deeply embedded equiaxed dimples.

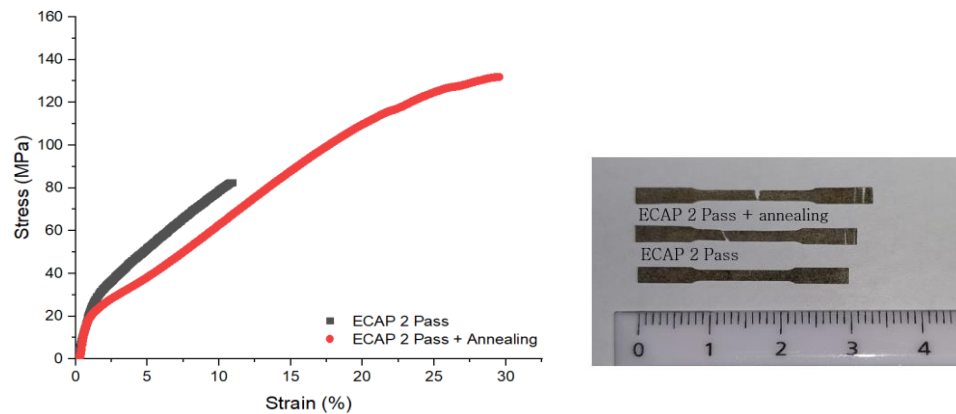


Figure 11. Comparison of the mechanical properties before and after annealing.

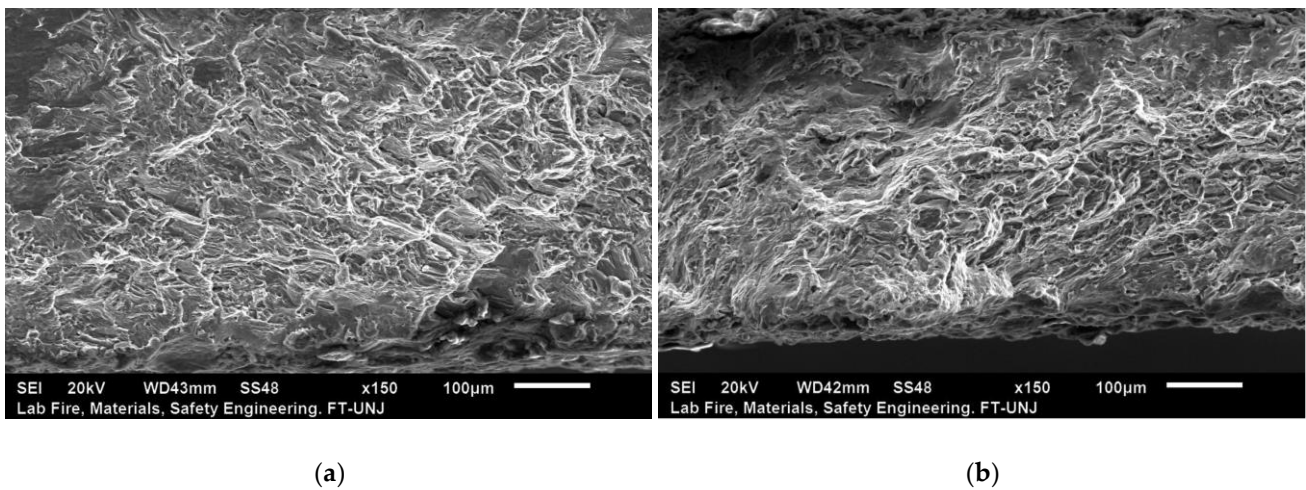


Figure 12. Tensile fracture of ECAP two-pass (a) before and (b) after annealing.

In polycrystalline materials, corrosion tends to preferentially attack grain boundaries. This is because grain boundaries have less perfect atomic structures, resulting in higher energy levels compared to perfect crystals. Additionally, grain boundaries are prone to impurities. Corrosion testing on ECAP specimens was conducted using the potentiodynamic polarization method. The polarization curves of ECAP two-pass before and after annealing are shown in Figure 13. By correlating the grain size after the annealing process, smaller grain sizes exhibited increasing corrosion resistance compared to the others. However, the corrosion rate is not solely determined by grain size but also by crystallographic orientation.

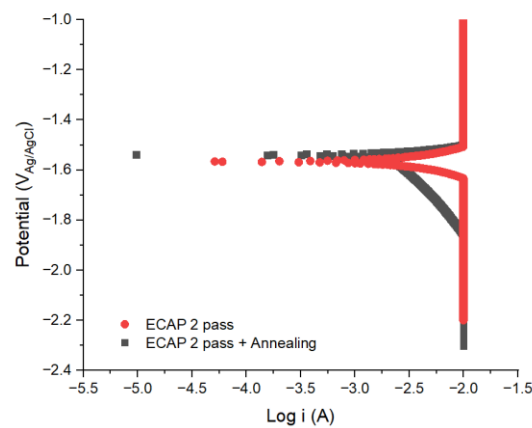


Figure 13. Polarization curve of ECAP magnesium before and after annealing (3.5% NaCl solution, $T = 37\text{ }^{\circ}\text{C}$).

Moreover, the tensile residual stress is eliminated through the heating process during annealing, resulting in a notable improvement in corrosion resistance from 13.91 to 6.53 mmpy. In accordance with the experiment by He et al., the annealing process has been found to significantly reduce the number of high-surface energy prismatic planes that are exposed to the sheet surface. As a result, the modified samples, with a symmetric weak basal texture, exhibited significantly enhanced corrosion resistance [31].

3.4. Microforming Application

The subsequent stage involved the testing phase in microforming, where the specimens underwent conditioning through the ECAP and annealing process. Figure 14 illustrates the deformation occurring during the blanking process of ECAP two-pass magnesium with a punch length function. At a punch depth of 10–20%, as shown in Figure 14a,b, plastic deformation equivalent to 10% of the plate thickness occurs. Subsequently, as the force exerted by the machine continues to increase, fracture occurs at a punch depth of 30%, as depicted in Figure 14c.

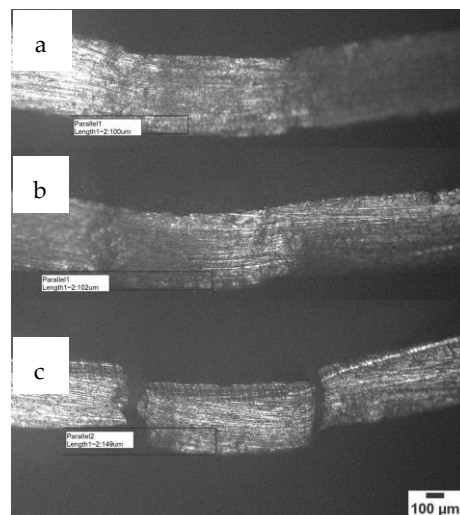


Figure 14. Deformation in the micro-blanking process of ECAP two-pass magnesium with a punch depth function (a) 10%, (b) 20%, and (c) 30% sheet thickness.

Unlike conventional processes involving ductile fracture mechanisms with crack initiation and propagation, in this microforming process utilizing a plate thickness of 0.5 mm, the crack region on the sheared edge is not clearly visible. The phenomenon is

primarily dominated by shear deformation, and crack initiation and propagation only become apparent shortly before the final fracture stage.

The smooth zone occurs due to the sliding between the workpiece and the scrap, as well as between the punch or die wall. A significant increase in ductility during the ECAP process will enhance the proportion of roll-over and smooth zone in the blanking process. Figure 15 illustrates that with the increased ductility resulting from annealing, the roll-over increases from 11% in ECAP two-pass to 14% in ECAP two-pass that has been annealed with a punch depth of 2.5 mm.

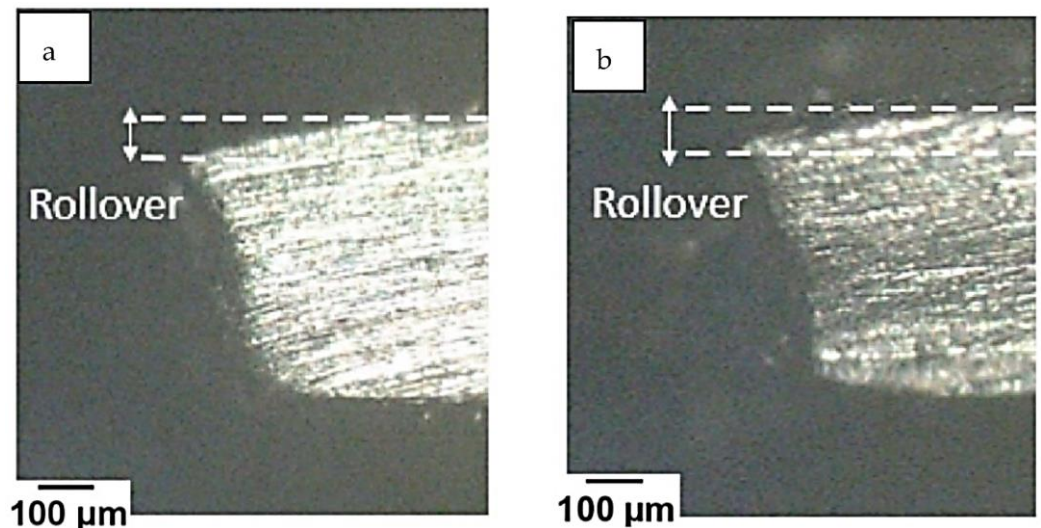


Figure 15. The roll-over of blanking process on (a) ECAP two-pass and (b) after annealing.

The observations of the fracture in ECAP two-pass and annealed ECAP two-pass shortly after fracture formation at a punch depth of 0.17 mm (30% thickness) are shown in Figure 16. It can be observed that the surface of the ECAP two-pass fracture forms a smooth zone with a height of 4% of the plate thickness, resulting from plastic deformation during the blanking process and material displacement prior to fracture.

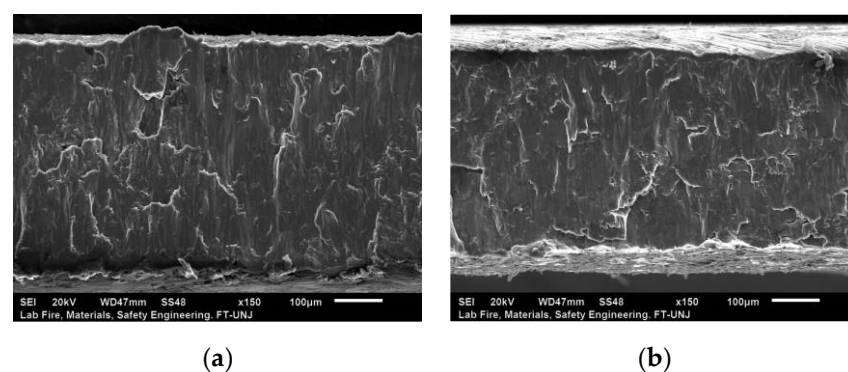


Figure 16. The sheared edge surface: (a) ECAP two-pass, (b) annealing ECAP two-pass.

In contrast, the fracture surface of the annealed ECAP two-pass exhibits an increased proportion of the smooth zone, reaching 12%. As explained earlier, this is associated with increased ductility after annealing, rising from 11% to 30%. However, the formation of the smooth zone is also influenced by clearance and punch velocity, and in this experiment, a clearance of 10 μm and a punch velocity of 7 mm/s were used. The smaller smooth zone value in Figure 16 than the roll-over in Figure 15 is due to the influence of the punch depth.



Figure 17 displays the microforming product, a miniplate made of ECAP magnesium. Corrosion testing in a 0.9% NaCl solution reveals that the miniplate exhibits the highest

corrosion resistance in ECAP two-pass, which has the smallest grain size. However, the miniplate produced through ECAP six-pass dissolves completely within one day when immersed in the NaCl solution. Corrosion resistance is also influenced by the texture, where the as-received magnesium, having a strong texture, demonstrates higher corrosion resistance than ECAP six-pass as shown in Table 4.



Figure 17. Miniplate product from microforming process.

Table 4. Duration of immersion until miniplate fractures.

Number of ECAP Pass	Grain Size (μm)	Duration of Immersion until Miniplate Fractures (Days)	Δ Mass (g)	pH	Corroded Miniplate
0	632	2	0.006	10.55	
2	115	5	0.004	10.38	
6	132	<1	0.029	10.48	completely dissolved

4. Conclusions

The severe plastic deformation involved in the ECAP process leads to significant grain refinement. The ECAP process, particularly with multiple passes, results in the formation of fine grains, improved grain distribution, and mechanical properties. While the increase in strength is modest, there is a notable increase in ductility, particularly in specimens with eight passes. Annealing after the ECAP process results in improved mechanical properties, including increased strength and ductility, and homogeneity.

In microforming applications, the ECAP process, combined with annealing, enhances the proportion of the roll-over and smooth zone during the blanking process. Increased ductility resulting from annealing contributes to a greater proportion of the smooth zone, improving the overall performance of the microforming process. Further research can explore the optimization of process parameters, such as the number of ECAP passes and annealing conditions, to achieve the desired outcomes in microforming applications. Overall, the combination of the ECAP process and annealing holds promise for enhancing a homogeneous grain distribution, controlling size effects, and producing high-quality microforming products.

Author Contributions: Conceptualization, G.K. and S.S.; methodology, S.S. and S.T.D.; validation, G.K., S.S. and S.T.D.; formal analysis, G.K. and S.S.; investigation, S.T.D.; resources, S.S.; data curation, S.T.D.; writing—original draft preparation, S.T.D.; writing—review and editing, G.K. and S.S.; visualization, S.T.D.; supervision, G.K. and S.S.; project administration, S.T.D.; funding acquisition, G.K. All authors have read and agreed to the published version of the manuscript.

Funding: This research was funded by the Penelitian Dasar Unggulan Perguruan Tinggi, Ministry of Education, Culture, Research and Technology, grant number: NKB-196/UN2.RST/HKP.05.00/2021.

Data Availability Statement: The data presented in this study are available in the article.

Acknowledgments: We are grateful to the Ministry of Education, Culture, Research, and Technology as well as to the Universitas Indonesia, for their significant contribution.

Conflicts of Interest: The authors declare no conflict of interest.

References

1. Chen, Q.; Thouas, G.A. Metallic implant biomaterials. *Mater. Sci. Eng.* **2015**, *87*, 1–57. [[CrossRef](#)]
2. Hermawan, H. Updates on the research and development of absorbable metals for biomedical applications. *Prog. Biomater.* **2018**, *7*, 93–110. [[CrossRef](#)]
3. Waizy, H.; Seitz, J.M.; Reifenrath, J.; Bach, F.W. Biodegradable magnesium implants for orthopedic applications. *J. Mater. Sci.* **2012**, *48*, 39–50. [[CrossRef](#)]
4. Agarwal, S.; Curtin, J.; Duffy, B.; Jaiswal, S. Biodegradable magnesium alloys for orthopaedic applications: A review on corrosion, biocompatibility and surface modifications. *Mater. Sci. Eng. C* **2016**, *68*, 948–963. [[CrossRef](#)] [[PubMed](#)]
5. Radha, R.; Sreekanth, D. Insight of magnesium alloys and composites for orthopedic implant applications—A review. *J. Magnes. Alloys* **2017**, *5*, 286–312. [[CrossRef](#)]
6. Brar, H.S.; Platt, M.O.; Sarntinoranont, M.; Martin, P.I.; Manuel, M.V. Magnesium as a biodegradable and bioabsorbable material for medical implants. *JOM* **2009**, *61*, 31–34. [[CrossRef](#)]
7. Zheng, Y.F.; Gu, X.N.; Witte, F. Biodegradable metals. *Mater. Sci. Eng.* **2014**, *77*, 1–34. [[CrossRef](#)]
8. Tekumalla, S.; Seetharaman, S.; Almajid, A.; Gupta, M. Mechanical Properties of Magnesium-Rare Earth Alloy Systems: A Review. *Metals* **2014**, *5*, 1–39. [[CrossRef](#)]
9. Cordero, Z.C.; Knight, B.E.; Schuh, C.A. Six Decades of the Hall–Petch Effect—A Survey of Grain-Size Strengthening Studies on Pure Metals. *Int. Mater. Rev.* **2016**, *61*, 495–512. [[CrossRef](#)]
10. Tong, L.B.; Chu, J.H.; Jiang, J.H.; Kamado, S.; Zheng, M.Y. Ultra-fine grained Mg-Zn-Ca-Mn alloy with simultaneously improved strength and ductility processed by equal channel angular pressing. *J. Alloys Compd.* **2019**, *785*, 410–421. [[CrossRef](#)]
11. Ralston, K.D.; Fabijanic, D.; Birbilis, N. Effect of Grain Size on Corrosion: A Review. *Corrosion* **2010**, *66*, 075005–075005-13. [[CrossRef](#)]
12. Zhang, J.; Peng, P.; She, J.; Jiang, B.; Tang, A. A study of the corrosion behavior of AZ31 Mg alloy in depth direction after surface nanocrystallization. *Surf. Coat. Technol.* **2020**, *396*, 125968. [[CrossRef](#)]
13. Faraji, G.; Kim, H.S.; Kashi, H.T. *Severe Plastic Deformation: Methods, Processing and Properties*; Elsevier: Amsterdam, The Netherlands, 2018; pp. 19–33.
14. Prithivirajan, S.; Naik, G.M.; Narendranath, S.; Desai, V. Recent progress in equal channel angular pressing of magnesium alloys starting from Segal’s idea to advancements till date—A review. *Int. J. Lightweight Mater. Manuf.* **2023**, *6*, 82–107. [[CrossRef](#)]
15. Poggiali, F.; Silva, C.; Pereira, P.H.; Figueiredo, R.; Cetlin, P. Determination of mechanical anisotropy of magnesium processed by ECAP. *J. Mater. Res. Technol.* **2014**, *3*, 331–337. [[CrossRef](#)]
16. Geiger, M.; Kleiner, M.; Eckstein, R.; Tiesler, N.; Engel, U. Microforming. *CIRP Ann.* **2001**, *50*, 445–462. [[CrossRef](#)]
17. Boljanovic, V. *Sheet Metal Forming Processes and Die Design*; Industrial Press: New York, NY, USA, 2014; pp. 43–50.
18. Myint, P.W.; Hagihara, S.; Tanaka, T.; Taketomi, S.; Tadano, Y. Determination of the Values of Critical Ductile Fracture Criteria to Predict Fracture Initiation in Punching Processes. *J. Manuf. Mater. Process.* **2017**, *1*, 12.
19. Engel, U.; Rosochowski, A.; Geißdörfer, S.; Olejnik, L. *Microforming and Nanomaterials*; Springer: Paris, France, 2007; pp. 99–124.
20. Wu, H.-Y.; Hsu, W.-c. Tensile flow behavior of fine-grained AZ31B magnesium alloy thin sheet at elevated temperatures. *J. Alloys Compd.* **2010**, *493*, 590–594. [[CrossRef](#)]
21. Kim, W.J.; Yoo, S.J.; Kim, H.K. Superplastic microforming of Mg–9Al–1Zn alloy with ultrafine-grained microstructure. *Scr. Mater.* **2008**, *59*, 599–602. [[CrossRef](#)]
22. Su, Q.; Xu, J.; Wang, C.; Shan, D.; Guo, B. The Fabrication of Micro-Array Channels with the Ultrafine-Grained LZ91 Mg-Li Alloy by Micro-Embossing. *Micromachines* **2018**, *9*, 55. [[CrossRef](#)]
23. Kiswanto, G.; Supriadi, S.; Dwiyati, S.T. Challenge in magnesium microforming. *IOP Conf. Ser. Mater. Sci. Eng.* **2021**, *1070*, 12121. [[CrossRef](#)]
24. Biswas, S.; Dhinwal, S.S.; Suwas, S. Room-temperature equal channel angular extrusion of pure magnesium. *Acta Mater.* **2010**, *58*, 3247–3261. [[CrossRef](#)]
25. Zhu, S.Q.; Yan, H.G.; Chen, J.H.; Wu, Y.Z.; Su, B. Feasibility of high strain-rate rolling of a magnesium alloy across a wide temperature range. *Scr. Mater.* **2012**, *67*, 404–407. [[CrossRef](#)]
26. Song, B.; Pan, H.; Chai, L.; Guo, N.; Zhao, H.; Xin, R. Evolution of gradient microstructure in an extruded AZ31 rod during torsion and annealing and its effects on mechanical properties. *Mater. Sci. Eng. A* **2017**, *689*, 78–88. [[CrossRef](#)]
27. Murphy, A.D.; Allison, J.E. The Recrystallization Behavior of Unalloyed Mg and a Mg–Al Alloy. *Metall. Mater. Trans. A Phys. Metall. Mater. Sci.* **2018**, *49*, 1492–1508. [[CrossRef](#)]
28. Indhiarto, I.; Shimizu, T.; Furushima, T.; Yang, M. Effect of DC pulsed-current on deformation behavior of magnesium alloy thin sheets. *Procedia Manuf.* **2018**, *15*, 1663–1670. [[CrossRef](#)]

29. Mahmudah, A.; Kiswanto, G.; Priadi, D. Fabrication of punch and die of micro-blanking tool. *IOP Conf. Ser. Mater. Sci. Eng.* **2017**, *215*, 012040. [[CrossRef](#)]
30. Hakimian, H.; Sedighi, M.; Asgari, A. Experimental and numerical study on the ECARed magnesium AZ31 alloy. *Mech. Ind.* **2015**, *17*, 110. [[CrossRef](#)]
31. He, J.; Jiang, B.; Xu, B.; Zhang, J.; Yu, X. Effect of texture symmetry on mechanical performance and corrosion resistance of magnesium alloy sheet. *J. Alloys Compd.* **2017**, *723*, 213–224. [[CrossRef](#)]

Disclaimer/Publisher's Note: The statements, opinions and data contained in all publications are solely those of the individual author(s) and contributor(s) and not of MDPI and/or the editor(s). MDPI and/or the editor(s) disclaim responsibility for any injury to people or property resulting from any ideas, methods, instructions or products referred to in the content.